Structural and electronic properties of $LaMnO_3$ under pressure: An *ab initio* LDA+U study

G. Trimarchi and N. Binggeli
INFM DEMOCRITOS National Simulation Center and Abdus Salam International Center for Theoretical Physics, Strada Costiera 11, 34014 Trieste, Italy

(Received 27 June 2004; revised manuscript received 27 September 2004; published 4 January 2005)

The structural and electronic properties of $LaMnO_3$ under hydrostatic pressure are investigated by means of *ab initio* LDA+U calculations, based on ultrasoft pseudopotentials. Previous theoretical studies have indicated that the local-density approximation (LDA) incorrectly predicts the ambient-pressure *Pnma* structure of $LaMnO_3$ to be metallic and significantly underestimates its Jahn-Teller distortion, when full structural optimization is performed. We find that the LDA+U approach corrects such features and provides a good general description of the complex structural changes observed in the $LaMnO_3$ *Pnma* phase under pressure. Consistent with experiment, we find that the off-center shift in the La *x* coordinates, present at low pressure, disappears at about 15 GPa. Our results indicate that this reduces the stability of the type-*d* Jahn-Teller distortion, giving rise to type-*a* and type-*d* Jahn-Teller distorted structures which are essentially degenerate in energy above ~15 GPa. We suggest that this may be a key element in driving the structural transition of the *Pnma* phase that is observed experimentally at ~15 GPa.

DOI: 10.1103/PhysRevB.71.035101 PACS number(s): 61.50.Ks, 71.20.Be, 71.20.Eh

I. INTRODUCTION

Recently considerable experimental and theoretical efforts have been devoted to the study of perovskite manganites with general formula $R_xA_{1-x}MnO_3$ $(0 \leqslant x \leqslant 1)$, where *R* is a rare earth atom (e.g., La, Pr, Nd) and *A* is an alkaline atom (e.g., Ca, Sr, Ba).[1] These materials exhibit puzzling physical properties related to a complex interplay between orbital, magnetic, charge, and structural degrees of freedom. This includes colossal-magnetoresistance (CMR) effects, and a large variety of phases with remarkably different structural, magnetic, and transport properties. The latter may be controlled, e.g., using doping, temperature, magnetic field, electric field, photoexcitation, chemical pressure, and/or external pressure.[2–4] The application of hydrostatic pressure (or strain), in particular, is a straightforward way to monitor the effect of the atomic structure on the electronic and magnetic properties.

Among the manganese oxides, $LaMnO_3$ is important because it is the *parent* system in the family of manganites that show the CMR effect. For this reason it is desirable to achieve a good understanding of its properties. At ambient condition, the MnO_6 octahedra in $LaMnO_3$ are strongly tilted with respect to the ideal cubic perovskite structure, and also significantly distorted by a collective Jahn-Teller (JT) effect. In recent years, the structure of this material has been studied under hydrostatic pressure using both neutrons[5] (up to 8 GPa, at room temperature and low temperature) and synchrotron x-ray diffraction techniques[6,7] (up to 40 GPa, at room temperature). These studies show that $LaMnO_3$ undergoes complex structural changes under pressure, both in its lattice parameters and internal atomic structure. Loa *et al.*[6] have carried out an x-ray refinement analysis and determined the internal atomic structure for the low pressure *Pnma* phase up to a pressure of 11 GPa; on the basis of a linear extrapolation of their data they propose that the JT distortion vanishes at ~18 GPa. More recently, Sani *et al.*[7] have detected a structural transition to a high-pressure phase at ~15 GPa. Concerning this phase, they find that above 15 GPa, an *Imma* structure (no JT distortion) provides a better fit to the high-pressure x-ray diffraction data than the *Pnma* structure. Raman[6] and neutron[5] data also suggest a structural transformation (to an unknown phase), but at a somewhat lower pressure. The neutron diffraction study[5] shows also that the low-temperature antiferromagnetic structure of the type *A* (AF-*A*), that is observed at ambient pressure, is stable up to at least 7 GPa. Furthermore, measurements of resistivity reveal that the system keeps its insulating nature at room temperature up to 32 GPa,[6] where it undergoes an insulator-metal transition.

The driving mechanisms behind the complex structural changes and the structural transition occurring in $LaMnO_3$ under pressure are presently far from being fully understood. The atomic structure of the insulating phase above 15 GPa is also still an open issue. To our knowledge no *ab initio* calculation has been carried out so far to investigate the pressure behavior of $LaMnO_3$. Calculations based on the density functional theory (DFT) within the local density approximation (LDA) and within the general gradient approximation (GGA) have addressed the electronic structure of $LaMnO_3$ using the experimental equilibrium structural parameters. Such calculations were able to reproduce the insulating band structure of $LaMnO_3$ at ambient (experimental) conditions. Previous theoretical work, however, also showed that when the internal atomic structure is fully relaxed, both LDA and GGA incorrectly predict the *Pnma* phase to be metallic,[8] and significantly underestimate its Jahn-Teller distortion. In the present work, we therefore address the properties of the *Pnma* phase using the LDA plus on-site-Coulomb-interaction approach (LDA+U), which is expected to fix the LDA/GGA band gap problem (see Ref. 8).

It is worth noticing that even though the LDA+U *ab initio* method has been introduced in the early 1990s, it has been used successfully mostly in studies of electronic struc-

tures, whereas it has been rarely applied to the optimization of atomic geometries. The present work therefore also aims at addressing the predictive capability of the LDA+U approach for structural properties. In a previous work, Sawada *et al.*[8] have used the LDA+U method together with the plane-wave pseudopotential scheme to optimize the internal atomic structure of $LaMnO_3$, keeping fixed the lattice parameters to the experimental ambient-pressure values. Here, we use a similar approach, but carry out full structural optimization of *Pnma* $LaMnO_3$ at constant pressure in order to examine the changes in the atomic and electronic structure as a function of pressure.

The paper is organized as follows: in Sec. II, we give some technical details on our LDA+U calculations; in Sec. III, the results for the atomic structure at zero pressure and under pressure are described and compared to experiment; in Sec. III D we examine the electronic structure of $LaMnO_3$ under pressure; the last section is devoted to the final remarks and to the conclusions.

II. COMPUTATIONAL METHOD

The calculations reported in this paper are performed within the LDA+U scheme using Vanderbilt ultrasoft pseudopotentials[9] and a plane-wave-basis set for the electronic orbitals. The LDA+U energy functional reads

$$E_{\mathrm{LDA+U}} = E_{\mathrm{LDA}} + E_{\mathrm{U}}, \tag{1}$$

where E_{LDA} is the DFT energy functional treated within the local-spin-density approximation[10] and E_{U} is the rotational invariant[11] on site correction[8,12,13]

$$E_{\mathrm{U}}[\{n^{I\sigma}_{mm'}\}] = \frac{U}{2}\sum_{I}\sum_{m\sigma}\left\{n^{I\sigma}_{mm} - \sum_{m'\sigma} n^{I\sigma}_{mm'} n^{I\sigma}_{m'm}\right\}$$

$$= \frac{U}{2}\sum_{I\sigma}\mathrm{Tr}[n^{I\sigma}(1-n^{I\sigma})]. \tag{2}$$

In this expression, $n^{I\sigma}$ is the occupation matrix of the localized 3*d* electron orbitals on the Mn site *I*, *U* is the effective Coulomb interaction between the localized *d* electrons and *m* and σ are orbital and spin indices, respectively. Within the ultrasoft pseudopotential scheme, the occupation matrix $n^{I\sigma}$ reads

$$n^{I\sigma}_{mm'} = \sum_{\mathbf{k},n} f_{\mathbf{k},n}\langle\psi^{\sigma}_{\mathbf{k},n}|\hat{S}|\phi^{I}_{m,\mathbf{k}}\rangle\langle\phi^{I}_{m',\mathbf{k}}|\hat{S}|\psi^{\sigma}_{\mathbf{k},n}\rangle, \tag{3}$$

where $\hat{S}$ is the overlap operator used to account for the augmentation charge,[9] $\psi^{\sigma}_{\mathbf{k},n}$ are the crystal pseudo-wavefunctions (**k** and *n* are, respectively, the **k** point and band indices), and $f_{\mathbf{k},n}$ are the corresponding occupation numbers. The orbitals $\phi^{I}_{m,\mathbf{k}}$ are Bloch sums of localized Mn 3*d* atomic (pseudo) orbitals ϕ^{I}_{m} sitting on ionic sites translationally equivalent to the Mn site *I*:

$$\phi^{I}_{m,\mathbf{k}} = \frac{1}{\sqrt{N}}\sum_{\mathbf{R}} e^{-i\mathbf{k}\cdot(\mathbf{R}+\tau_I)}\phi_m(\mathbf{r}-\mathbf{R}-\tau_I), \tag{4}$$

where the sum runs over the lattice vectors, **R**, and τ_I is the position of the Mn site *I*. The quantity E_{U} in Eq. (2), is positive definite ($U>0$), as the eigenvalues of the on-site occupation matrix have values between 0 and 1. This contribution to the LDA+U energy functional may be viewed as a penalty term that favors integer occupations of the localized orbitals (in our case the Mn *d* orbitals).

The value of the *U* parameter in Eq. (2) has been calculated following the LDA linear-response approach proposed by Cococcioni and de Gironcoli,[13,14] inspired by the perturbative scheme by Pickett *et al.*[15] We point out that the approach we employ here to evaluate U is internally consistent[13] with the implementation of the LDA+U we use, in particular with our choice of localized orbitals, i.e., pseudoatomic orbitals. Using the experimental equilibrium values of the structural parameters of $LaMnO_3$, we obtain $U=4.5$ eV, which is the value we will use in the present work. We note that we have recalculated *a posteriori* the value of U for the atomic structure we obtain at high pressure ($P\approx 15$ GPa) and find that U changes (decreases) by no more than 15%. Such a change is expected to have a minor influence on the structural properties, and is neglected here (see also Ref. 16).

The ultrasoft pseudopotentials have been constructed using the following reference atomic configurations: La, $[\mathrm{Xe}]5s^2 5p^6 5d^1 6s^2 4f^0$; O, $[\mathrm{He}]2s^2 2p^4$; and Mn, $[\mathrm{Ar}]3d^5 4s^2$ (see Ref. 17 for the parameters used to produce the pseudopotentials). For manganese we have used the nonlinear-core correction: this has been shown[18] to be important to reproduce in a satisfactory way the properties of materials containing magnetic ions such as Mn, Fe, or Co. The kinetic energy cutoff we use for the plane-wave expansion of the electronic states is 35 Ry; a cutoff of 280 Ry is used for the electronic density. The sampling of the Brillouin zone (BZ) is carried out with a grid (4,4,2) of the Monkhorst-Pack kind and we use a Gaussian smearing of the electronic levels, with full width at half maximum of $\sigma=0.005$ Ry, to determine the Fermi energy.

In the present work, we focus on the $T=0$ K magnetic-ordered AF-*A* configuration of the system. The experiments in Refs. 6 and 7 were both performed at room temperature, i.e., in the paramagnetic (PM) state (the Néel temperature is $\sim$140 K). It should be noted, however, that there is no significant difference between the experimental structural properties of the insulating PM and AF-*A* phase at ambient pressure (see, e.g., Ref. 19). Furthermore, previous LDA+U calculations performed for a similar perovskite system: $KCuF_3$ (see Ref. 20), indicate that the magnetic order (AF-*A*, AF-*C*, AF-*D*, ferromagnetic) has virtually no influence on the atomic structure and, in particular, on the Jahn-Teller distortion. Hence, we expect the AF-*A* and PM phases to also exhibit similar structural trends under pressure. In this connection, we would like to note that using a fictious nonmagnetic configuration to model the electronic and structural properties of the PM phase is known, instead, not to be a good approximation for transition-metal oxides and related compounds.[21–24] Indeed, unlike the magnetic-ordered structures[19,22] (and the PM structure[22,25]), this type of configuration does not satisfy Hund's rule.[21]

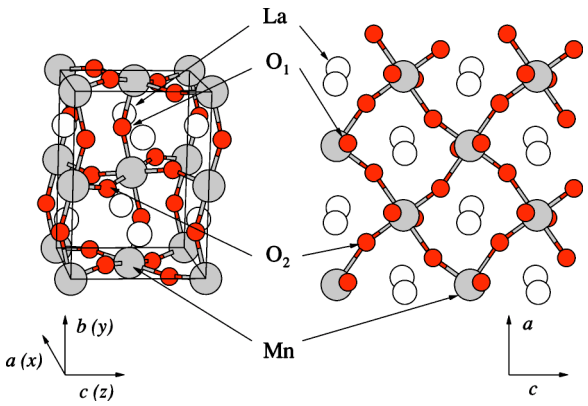

FIG. 1. (Color online) Crystal structure of $LaMnO_3$ with the *Pnma* symmetry. The unit cell (left) and the projection of the atomic structure in the *ac* plane (right) are displayed. The oxygen ions of the basal plane of the octahedron are labeled as O_2 (see Table I with the Wyckoff positions); they are characterized by two different O-Mn bond lengths [long (l) and short (s)]. The oxygen O_1 ions, instead, are characterized by two identical O-Mn bond lengths [medium (m)].

III. STRUCTURAL PROPERTIES OF $LaMnO_3$

A. Introductory remarks

At ambient condition, $LaMnO_3$ has the $GdFeO_3$-like orthorombic structure with *Pnma* symmetry (see Ref. 26 for the experimental structural parameters). In Fig. 1, the atomic structure of this material is illustrated: it contains a network of corner sharing MnO_6 octahedra. This structure can be obtained from the standard cubic perovskite structure by two subsequent rotations of the MnO_6 octahedra, namely (i) around the *b* axis and (ii) around the *a* axis of the final *Pnma* orthorombic cell. It is worth noticing that considering only the latter rotation and neglecting the Jahn-Teller distortion (see later) the distorted structure would have the orthorhombic *Imma* symmetry. The MnO_6 octahedra in $LaMnO_3$ are cooperatively distorted due to the Jahn-Teller instability of the Mn^{3+} ions. Using, for the sake of simplicity, an atomic-like picture, every Mn^{3+} ion is in a high spin d^4 configuration with three electrons occupying the three t_{2g} orbitals and one electron in an e_g orbital. The cooperative Jahn-Teller distortion releases the degeneracy of e_g orbitals, that would originate from the local cubic environment of the Mn ion, and leads to different Mn-O bond lengths. The $x(x=u-1/2)$ and $z(z=v)$ Wyckoff coordinates of the lanthanum atoms (see Table I with the Wyckoff positions and Table III with their experimental values at zero pressure) are different from zero: this off-center shift is related to the tilting of the oxygen octahedra, and allows the La atoms to become more nearly equidistant from the neighboring oxygen atoms.[27] The structural optimization needed to determine the optimal lattice parameters and the behavior of the material under hydrostatic pressure has been carried out taking several different unit-cell volumes *V*, and for each volume optimizing the values of a/b and c/b with fully relaxed internal atomic structures. For each *V*, a/b, and c/b, the calculated forces on the atoms do not exceed 10^{-3} Ry/a.u., and the stress matrix is diagonal and has identical diagonal elements to within 5 kbar. This corresponds to errors in both the atomic positions and lattice parameters of about two parts per thousands. A third-order Birch-Murnaghan equation of state has been used to evaluate the equilibrium volume, the bulk modulus B_0, and its first pressure derivative B'. Within this approach we control the volume, whereas the pressure for each value of the volume is evaluated *a posteriori* using the Birch-Murnaghan equation fit to the curve of the total energies as a function of volume.

TABLE I. The Wyckoff positions for each ionic specie in the *Pnma* structure of $LaMnO_3$.

Atom	Class	Coordinates
La, O_1	4*c*	$(u,1/4,v)$, $(\bar{u}+1/2,3/4,v+1/2)$
		$(\bar{u},3/4,\bar{v})$, $(u+1/2,1/4,\bar{v}+1/2)$
Mn	4*a*	(0, 0, 0), (1/2,0,1/2)
		(0,1/2,0), (1/2,1/2,1/2)
O_2	8*d*	$\pm(x,y,z)$
		$\pm(\bar{x},\bar{y},z)+(1/2,0,1/2)$
		$\pm(\bar{x},y,\bar{z})+(0,1/2,0)$
		$\pm(x,\bar{y},\bar{z})+(1/2,1/2,1/2)$

B. Properties at $P=0$ and equation of state

We discuss now the results of the optimization of the *Pnma* structure at zero pressure. In Table II, we present some geometrical parameters characterizing the relaxed internal structure obtained both within the LDA+U and within the LDA, using the experimental values of the lattice parameters at ambient pressure (the corresponding Wyckoff atomic positions are reported in Table III). The results are compared to experiment and previous calculations. Both LDA+U and LDA give a stable JT distortion, confirming the outcome of previous internal atomic relaxation calculations.[8] Within the LDA+U (LDA) the calculated relaxed bond lengths for the three inequivalent Mn—O bonds are 2.17 (2.16), 1.97 (1.96), and 1.93 (1.92) Å, compared to 2.18, 1.96, and 1.90 Å in the experiment. The values of the Q_2 and Q_3 normal modes of the JT distortion (see Table II for their definition) do not differ from the experimental one by more than 17%. The ionic relaxation carried out with LDA+U provides a slightly better value for Q_2 with respect to LDA, but worsens somewhat the value of Q_3. We notice also that the tilting of the octahedra is relatively well reproduced, even though the LDA+U gives slightly smaller angles, i.e., a slightly more tilted structure. This trend is found also in the structure under pressure. We note that the equilibrium internal atomic structure obtained in the present work is in better general agreement with experiment than found in previous work.[8] The differences are most likely due to differences in the pseudopotentials generation. We found, for example, that the production of the pseudopotential for lanthanum deserves particular care. In addition to the La 5*d* and 6*s* states, we found that it is important to treat also the semicore 5*p* states as valence states in order to properly describe the tilting of the octahedra in the relaxed structure.[28] We note that, consis-

TABLE II. Data for the internal atomic structure of *Pnma* $LaMnO_3$ obtained using the experimental equilibrium lattice parameters (Ref. 26) $a=5.742$ Å, $b=7.668$ Å, $c=5.532$ Å. The values of some important geometrical parameters characterizing the internal geometry are reported. The three inequivalent Mn-O distances are labeled: *l*, *s*, *m* for long, short, and medium, respectively. The angles θ_1 and θ_2 stand for the Mn-O_2-Mn and Mn-O_1-Mn angles, respectively. The local modes characterizing the cooperative Jahn-Teller effect in $LaMnO_3$ are $Q_2=2(l-s)/\sqrt{2}$ and $Q_3=2(2m-l-s)/\sqrt{6}$; the numbers in parentheses indicate the deviation with respect to the experimental value.

	Mn-O (Å)	Mn-O-Mn (°)	Q_2 (Å)	Q_3 (Å)
Experiment	(*l*)2.184	(θ_1)154.3	0.398	−0.142
	(*m*)1.957	(θ_2)156.7		
	(*s*)1.903			
LDA[a]	(*l*)2.156	(θ_1)155.5	0.329(−17%)	−0.127(10%)
	(*m*)1.961	(θ_2)155.5		
	(*s*)1.923			
LDA[b]	(*l*)2.099	(θ_1)157.0	0.189(−53%)	−0.124(13%)
	(*m*)1.956	(θ_2)157.0		
	(*s*)1.966			
LDA+U[a]	(*l*)2.168	(θ_1)153.5	0.341(−14%)	−0.120(15%)
	(*m*)1.974	(θ_2)152.2		
	(*s*)1.927			
LDA+U[b]	(*l*)2.110	(θ_1)158.0	0.221(−44%)	−0.124(13%)
	(*m*)1.956	(θ_2)157.0		
	(*s*)1.954			

[a]This work.
[b]From Ref. 8.

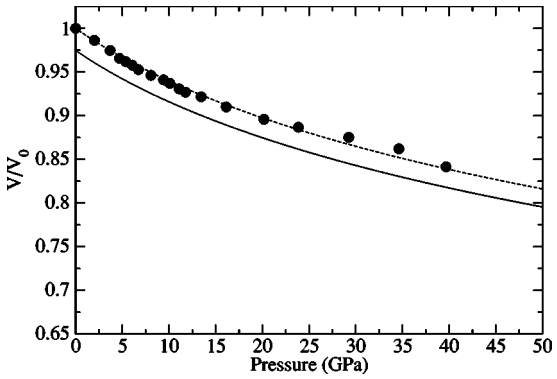

FIG. 2. Volume ratio V/V_0 vs pressure for $LaMnO_3$. Circles are the experimental data taken from Lao *et al.* (Ref. 6). The continuous line and the dashed line are the theoretical curves for the *Pnma* phase where, respectively, the volumes have been normalized to the zero-pressure experimental and theoretical volume.

tent with previous work[8,29] we find a small band gap within the LDA, when the experimental equilibrium structural parameters are used. However, as soon as the atomic structure is relaxed, the system becomes metallic and the JT distortion significantly decreases within the LDA.[30] Within the LDA+U, instead, the gap remains open, both with the experimental and theoretical equilibrium structural parameters.

The values of the $LaMnO_3$ equilibrium structural parameters obtained within the LDA+U are displayed in the Table III together with the experimental values. We also reported in this table the LDA+U values of the internal structural parameters calculated using the experimental lattice parameters, for comparison. The theoretical lattice parameters agree to within ~1% with the measured values. The full structural optimization leads to internal structural parameters which compare also quite well to experiment.

Let us now consider the calculated parameters of the equation of state. We report, in Fig. 2, the variation of the

TABLE III. The Wyckoff positions for the experimental cell and for the theoretical equilibrium cell of *Pnma* $LaMnO_3$.

Ion	*u*	*v*	*x*	*y*	*z*
Expt.[a]					
$a=5.742$ Å, $b=7.668$ Å, $c=5.532$ Å					
La	0.549	0.010			
O_1	−0.014	−0.070			
O_2			0.309	0.039	0.224
LDA+U, expt. cell					
La	0.553	0.010			
O_1	−0.015	−0.074			
O_2			0.303	0.039	0.224
LDA+U, optimized cell					
$a=5.675$ Å, $b=7.608$ Å, $c=5.50$ Å					
La	0.549	0.009			
O_1	−0.012	−0.081			
O_2			0.301	0.042	0.223

[a]From Ref. 26.

TABLE IV. Equation-of-state parameters for the *Pnma* phase of $LaMnO_3$. The theoretical parameters have been obtained fitting the Birch-Murnaghan equation to the total energy values obtained for the various volumes considered.

		V_0 (Å^3)	B_0 (GPA)	B'
Experiment	[a]		104	9.5
	[b]	244.11	108	8.5
	[c]	245.05		
Theory	LDA+U	237.46	133.0	6.1

[a]From Ref. 7.
[b]From Ref. 6.
[c]From Ref. 5.

volume with applied hydrostatic pressure of the *Pnma* phase. The theoretical curve agrees rather well with the experimental data. The LDA+U slightly underestimates (by 2.5%) the equilibrium volume (see Table IV); the theoretical bulk modulus B_0 is 133 GPa, i.e., within 28% of the experimental value obtained in Ref. 7 and within 23% of the one reported in Ref. 6. We are not aware of previous *ab initio* evaluation of B_0 for $LaMnO_3$, but for other strongly correlated systems[31] the LDA+U performs better than the LDA estimating it.

C. Structural properties as a function of pressure

Now we turn our attention to the structural properties of $LaMnO_3$ under pressure. In Fig. 3, the relative changes, under pressure, in the lattice parameters a, c, and $b/\sqrt{2}$ are presented. For each pressure reported, both the theoretical LDA+U and the experimental values of the cell-shape ratios a/a_c, c/a_c, and $(b/\sqrt{2})/a_c$ are shown using, respectively, as a reference the lattice parameter a_c of the ideal cubic perovskite that has the same volume. The calculated curves reproduce rather well the experimental trends at low pressure, i.e., below ~15 GPa. At higher pressures, the differences with respect to experiment become more significant; experimentally, $LaMnO_3$ has been reported[7] to transform to a new phase at ~15 GPa. In Fig. 4, we illustrate the pressure behavior obtained for the Mn-O distances and compare it to that derived from x-ray crystallography studies for pressures below 15 GPa (*Pnma* structure). Although the data are somewhat scattered, the reduction of the MnO(l) and MnO(m) bond lengths and the decrease in amplitude of the JT distortion are quite clear. The theoretical curves describe well these trends. The curve for the MnO(m) bond, closely reproduces the corresponding experimental values. Based on the experimental data in Fig. 4 the decrease in length of the MnO(l) bond is quite striking, but it is harder to assess whether the MnO(s) bond is increasing or decreasing under pressure. The static LDA+U calculations predict a slight decrease under pressure also for the MnO(s) bond. This is in agreement with the results of the refinement analysis carried out in the neutron diffraction study[5] for pressure up to 7 GPa. The theoretical curve for the MnO(l) bond length describes well the experimental data below 15 GPa. We note, however, that contrary to the proposed experimental extrapo-

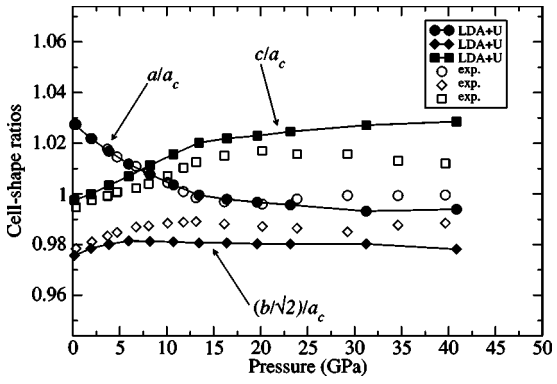

FIG. 3. Cell-shape ratios: a/a_c, c/a_c, and $(b/\sqrt{2})/a_c$ as a function of pressure for $LaMnO_3$; a_c is the lattice parameter of the ideal cubic perovskite cell with the same volume per formula unit. Open symbols are the experimental data taken from Loa *et al.* (Ref. 6), filled symbols are the *ab initio* results for the *Pnma* phase.

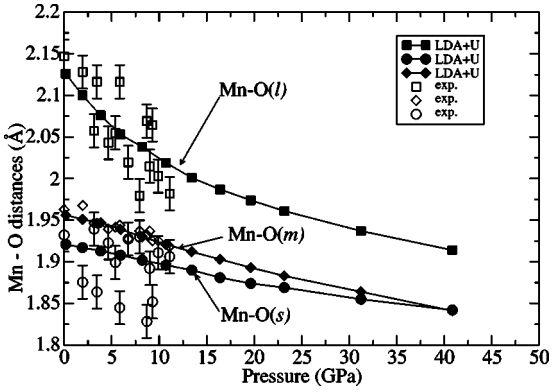

FIG. 4. Mn-O distances of the MnO_6 octahedra in $LaMnO_3$ as a function of the hydrostatic pressure. Open symbols are the experimental data from Loa *et al.* (Ref. 6) filled symbols are the *ab initio* results for the *Pnma* phase. Squares, circles, and diamonds refer, respectively, to the long (l) short (s), and medium (m) Mn-O distances.

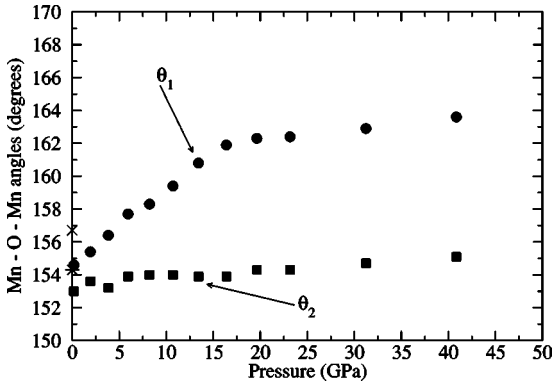

FIG. 5. Amplitude (in degrees) of the Mn-O_2-Mn angle θ_1 (circle) and of the Mn-O_1-Mn angle θ_2 (squares) as a function of pressure. The star and the cross markers at $P=0$ are the values respectively of θ_1 and θ_2 observed at ambient pressure in the experimental structure.

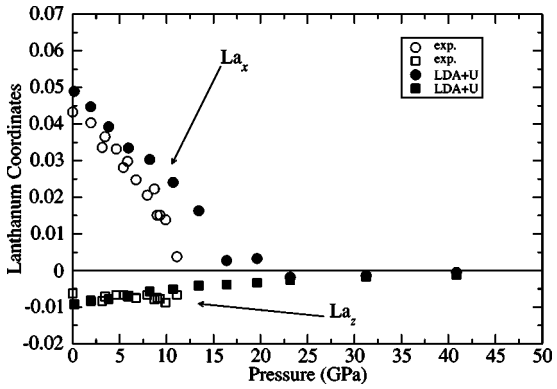

FIG. 6. x (circles) and z (squares) coordinates of La in $LaMnO_3$ as a function of pressure. Filled symbols refer to the theoretical results, open symbols refer to the experimental results of Ref. 6.

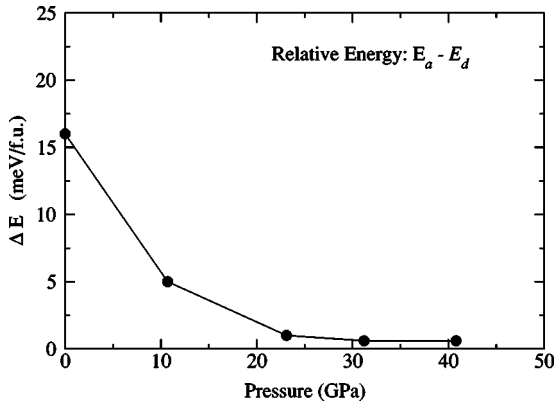

FIG. 7. Behavior with pressure of the difference ΔE between E_a, energy of the type-a JT, and E_d, energy of the type-d JT.

lation from data taken below 11 GPa,[6] our calculations indicate a nonlinear behavior of the MnO(l) bond length in the *Pnma* phase under pressure, and a nonvanishing JT distortion well above 18 GPa.

In Fig. 5, we report the changes of the angles θ_1 and θ_2, i.e., respectively the Mn-O_2-Mn and Mn-O_1-Mn angles. These angles are related to the tilting of the MnO_6 octahedra: their changes reflect the rotations of the octahedra under pressures. The value of θ_2 increases by just of few degrees up to ~7 GPa and then remains almost constant, while θ_1 increases steadily up to ~15 GPa. These changes lead to a configuration in which the octahedra are not tilted anymore about the y axis, and only the tilting about the x axis remains (see Fig. 8).

The changes in the x and z coordinates of La (that we will refer to as La_x and La_z, respectively) under pressure are reported in Fig. 6. The decrease in the tilting of the oxygen octahedra about the b axis is accompanied by a decrease in the La_x coordinate (x shift) to preserve the La—O distances. The decrease in La_x with increasing pressure that we find for the *Pnma* phase is consistent with the experimental trend, although the pressure at which La_x vanishes is somewhat higher in the calculation (17–20 GPa) than observed experimentally (12–15 GPa). We note that above 15 GPa, the x-ray structural refinements postulating an *Imma* phase yield $La_x=0$ (see Ref. 7), which is also what we obtain for the *Pnma* structure at high pressure (>20 GPa). The calculated z coordinate of La agrees well with the experimental data at low pressure (up to 12 GPa); at higher pressures, La_z is found to smoothly go to zero in the continuation of the *Pnma* phase.

Although the *Pnma* structure has been reported to transform to a different phase above 15 GPa, it is interesting to examine the high-pressure evolution of this structure in order to understand the possible origin of its loss of stability. In Fig. 8, we show the atomic structure we obtain for the *Pnma* phase at 40 GPa. The tilting of the O octahedra about the b axis has disappeared and the La cations exhibit a simple orthorombic packing with no La_x, La_z off-center shift (see also Fig. 1 for comparison). Such features are expected to

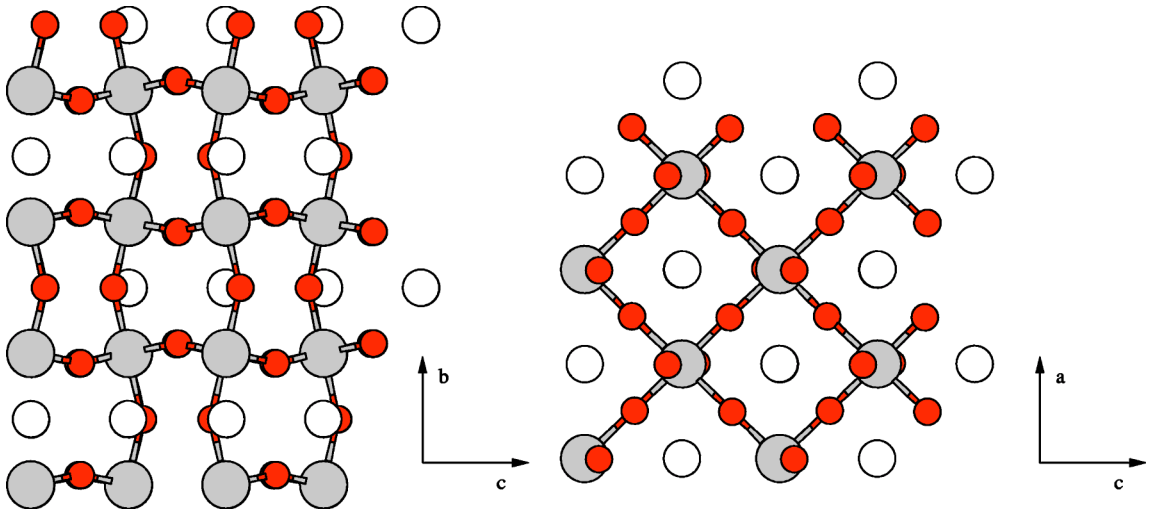

FIG. 8. (Color online) Atomic structure of the $LaMnO_3$ *Pnma* phase at high pressure. The projection in the b, c plane (left) and in the a, c plane (right) of the relaxed atomic structure at $P \approx 40$ GPa are displayed. Compared to the experimental structure at $P=0$ (Fig. 1), the off-center displacements of the lanthanum atoms vanish and the tilting of the oxygen octahedra around the b axis disappears in the *Pnma* phase at high-pressure.

derive from the increasing ionic character of the interactions at high pressure. The disappearance of the La off-center shift at pressures close to the experimental transition pressure ($\sim$15 GPa) is a feature which is observed both in our calculations and experimentally. We suggest that this feature may trigger the transformation observed experimentally. Indeed, previous theoretical work by Mizokawa *et al.*[32] has shown that, at ambient pressure, the La shift is essential to stabilize the type-*d* polytype structure of $LaMnO_3$ (the experimental low-pressure structure of $LaMnO_3$) with respect to the type-*a* polytype (found in other JT distorted perovskite systems). We have therefore investigated the relative stability of the type-*a* versus type-*d* (JT distorted) structures of $LaMnO_4$, which differ in the stacking of the MnO planes along the *b* axis.[32]

In Fig. 7, we show the dependence with pressure of the difference between the energies of the two JT distorted polytypes. Below 15 GPa, the type-*d* structure is significantly more stable than the type-*a* structure. However, above 15 GPa, when the La shift vanishes, the two structures are found to be essentially degenerate in energy ($\Delta E \lesssim 1$ meV/f.u.), within the accuracy of the LDA+U calculations. These results suggest that the disappearance of the La shift experimentally. Based on these results, we also suggest that the new phase may include a mixture of type-*a* and type-*d* stacking of the MnO planes. The resulting loss of the in-phase JT distortions of the O octahedra along the *b* axis may indeed be viewed, when averaging over the JT distorted sites along the *b* axis, as a globally (in average) vanishing JT distortion. This may explain the better fit to the high-pressure data, obtained in Ref. 7, postulating an *Imma* structure. Finally, we would like to mention, in this connection, that we have also carried out structural optimization starting from the structural parameters derived from the x-ray refinements for an *Imma* structure in Ref. 7 (at 16 GPa). In our calculations, however, this structure is metallic and unstable at pressures below $\sim$45 GPa, i.e., when symmetry constraints are removed it relaxes towards the *Pnma* structure. We note that when the JT distortion is artificially switched off in the *Pnma* phase (to produce the *Imma* structure, see Sec. III A) the system becomes metallic. It is actualy only at higher pressures ($\sim$45 GPa) when the *Pnma* structure itself becomes metallic (see next section), that we find its JT distortion to vanish, and recover the *Imma* (metallic) phase.

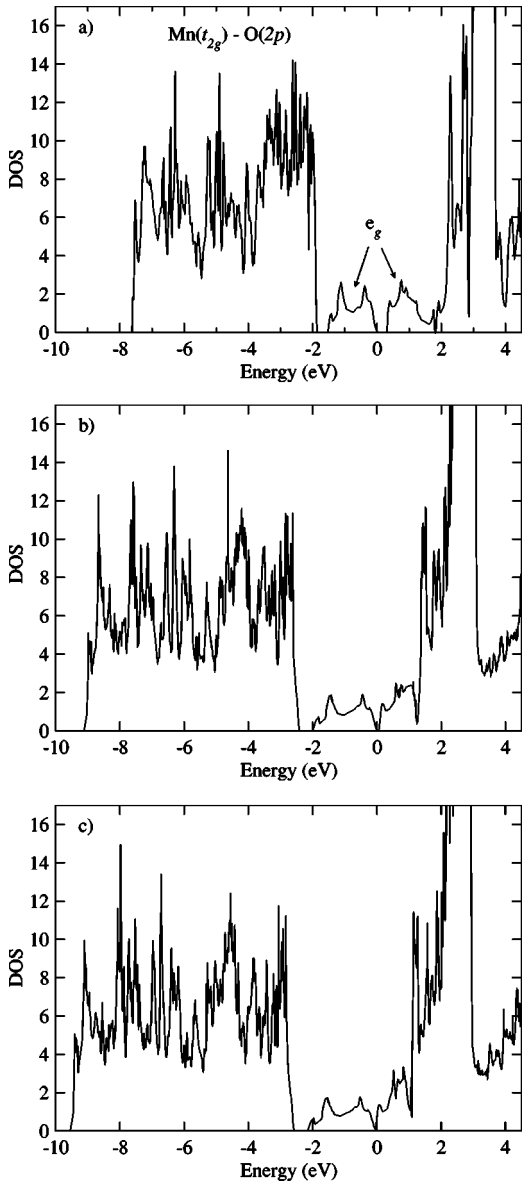

FIG. 9. Calculated DOS of $LaMnO_3$ at selected pressures. Going from the top to bottom panel, the DOS refers to structures with increasing pressures $P=6$, 31, 41 GPa. The valence band edge in panels (a) and (b), and the Fermi level in panel (c), respectively, have been chosen to be the zero of the energy scale.

D. Electronic structure

In Fig. 9, we report the total density of states (DOS) of *Pnma* $LaMnO_3$ at three different pressures: $P=6$, 31, 41 GPa. The DOS we obtain at low pressure (6 GPa) differs somewhat from previous calculated DOS obtained within the LDA/GGA using the experimental structural parameters at ambient pressure.[8,29,33] For the occupied states, the changes concern mainly the DOS structure between -1.5 and -8 eV. In the LDA/GGA calculations, this structure is split into a high-energy feature (-2.5 to -1.5 eV), containing mostly Mn t_{2g} states, and a low-energy structure (-7 to -2.5 eV), with mainly O_{2p} states. Within the LDA+U approach, the t_{2g} states are shifted at lower energy, within the O_{2p} bands,[34,35] giving rise to the DOS structure with three main peaks between -1.5 and -8 eV in Fig. 9(a). We note that compared to the measured photoemission spectrum[36] the agreement of our calculated LDA+U valence DOS is as good as—if not better than—that of previous calculated LDA valence DOSs.[36] At $P \approx 6$ GPa, the calculated band gap is $\sim$0.30 eV. Under pressure, due to the broadening of the bands, the gap decreases, and reaches a value of 0.05 eV at 31 GPa [Fig. 9(b)]. At 41 GPa, the system is clearly metallic [Fig. 9(c)]. We note that the actual insulator-metal transition of the experimental high-pressure phase occurs at $\sim$32 GPa, which is not dramatically different from the transition pressure we obtain for the *Pnma* insulator-metal transition.

IV. FINAL REMARKS AND CONCLUSIONS

In the present study, we have examined, using an *ab initio* LDA+U pseudopotential approach, the changes occurring in the structural and electronic properties of the *Pnma* phase of $LaMnO_3$ under hydrostatic pressure conditions. At ambient pressure, the LDA/GGA fails to correctly predict the insulating ground state of the $LaMnO_3$ *Pnma* structure and significantly underestimates its JT distortion, when full structural optimization is performed. The LDA+U corrects such features and describes well the complex structural changes of the *Pnma* phase under hydrostatic pressure. In particular, the relative changes in the *a*, *b*, and *c* lattice parameters are in good general agreement with experiments. We find that the off-center displacement of the La atoms, present at low pressure in the *Pnma* structure, vanishes at a pressure close to that observed experimentally ($\sim$15 GPa). This change is related to a change in the orientation of the MnO_6 octahedra: the tilting of the octahedra around the *b* axis disappears, and only the tilting around the *a* axis remains. These modifications reflect the natural evolution of the structure toward a configuration with close stacked oxygen (100) planes, compatible with the symmetries of the *Pnma* phase.

In a previous study, Mizokawa *et al.*[32] have shown that at ambient pressure, the La off-center displacement is essential to stabilize the observed type-*d* polystructure of $LaMnO_3$ with respect to the type-*a* structure. We have thus also investigated the relative stability of the type-*a* versus type-*d* structures under pressure. We find that the stability of the type-*d* structure, relative to the type-*a* structure, decreases under pressure, and that the two configurations become essentially degenerate in energy (within the accuracy of the LDA+U calculations) when the La displacement disappears above 15 GPa. We therefore suggest that the disappearance of the La shift may be a key element in driving the structural transition reported at $\sim$15 GPa, and that the new phase may include a mixture of type-*a* and type-*d* stacking of the MnO atomic planes. To further address the issue of the high-pressure phase, however, we note that it may be important to also take into account dynamical effects (including dynamical correlations, which are beyond the LDA+U).

ACKNOWLEDGMENTS

We would like to thank M. Altarelli for many fruitful discussions and a careful reading of the manuscript. We also acknowledge stimulating discussions with M. Cococcioni, S. Fabris, S. de Gironcoli, N. Stojic, and A. Callegari. We are grateful to C. Meneghini for sending us Ref. 7 prior to publication. We acknowledge support for this work by the INFM within the framework of the "Iniziativa Trasversale di Calcolo Parallelo." The calculations presented in this paper have been carried out using the PWSCF package.[37]

[1] E. Dagotto, *Nanoscale Phase Separation and Colossal Magnetoresistance* (Springer, New York, 2002).
[2] A. Asamitsu, Y. Tomioka, H. Kuwahara, and Y. Tokura, Nature (London) **388**, 50 (1997).
[3] M. Fiebig, K. Myano, Y. Tomioka, and Y. Tokura, Science **280**, 1925 (1998).
[4] M. Salamon and M. Jaime, Rev. Mod. Phys. **73**, 583 (2001).
[5] L. Pinsard-Gaudart, J. Rodriguez-Carvajal, A. Daoud-Aladine, I. Goncharenko, M. Medarde, R. I. Smith, and A. Revcolevschi, Phys. Rev. B **64**, 064426 (2001).
[6] I. Loa, P. Adler, A. Grzechnik, K. Syassen, U. Schwarz, M. Hanfland, G. K. Rozenberg, P. Gorodetsky, and M. P. Pasternak, Phys. Rev. Lett. **87**, 125501 (2001).
[7] A. Sani, C. Meneghini, S. Mobilio, S. Ray, D. D. Sarma, and J. A. Alonso (un published).
[8] H. Sawada, Y. Morikawa, K. Terakura, and N. Hamada, Phys. Rev. B **56**, 12154 (1997).
[9] D. Vanderbilt, Phys. Rev. B **41**, 7892 (1990).
[10] J. P. Perdew and A. Zunger, Phys. Rev. B **23**, 5048 (1981).
[11] A. Liechtenstein, V. Anisimov, and J. Zaanen, Phys. Rev. B **52**, R5467 (1995).
[12] S. L. Dudarev, G. A. Botton, S. Y. Savrasov, C. J. Humphreys, and A. P. Sutton, Phys. Rev. B **57**, 1505 (1998).
[13] M. Cococcioni and S. de Gironcoli, cond-mat/0405160 (unpublished).
[14] M. Cococcioni, Ph.D. thesis, SISSA, 2002.
[15] W. E. Pickett, S. C. Erwin, and E. C. Ethridge, Phys. Rev. B **58**, 1201 (1998).
[16] In order to check the influence of the value of U on the band structure, we have kept fixed the geometry optimized at 6 GPa and repeated the electronic structure calculation for a value of U different from the one used throughout the article (i.e., U =4.5 eV). In particular, we have considered the change of the band gap: taking U=4.0 eV the band gap changes from 0.30 to 0.27 eV.
[17] We report the cutoff radii used in the pseudopotential generation. For La we have r_c^s=2.2 a.u., r_c^p=2.0 a.u., r_c^d=2.2 a.u., and r_c^f =2.0 a.u. For Mn the radii are r_c^s=2.0 a.u., r_c^p=2.4 a.u., and r_c^d =1.8 a.u.. For O their value is r_c^s=1.3 a.u., r_c^p=1.3 a.u..
[18] E. G. Moroni, G. Kresse, J. Hafner, and J. Furthmuller, Phys. Rev. B **56**, 15629 (1997).
[19] J. Rodrìguez-Carvajal, M. Hennion, F. Moussa, A. H. Moudden, L. Pinsard, and A. Revcolevschi, Phys. Rev. B **57**, R3189 (1998).
[20] N. Binggeli and M. Altarelli, Phys. Rev. B **70**, 085117 (2004).
[21] V. A. Gubanov, A. I. Liechtenstein, and A. V. Postnokov, *Magnetism and the Electronic Structure of Crystals* (Springer-Verlag, Berlin, 1992).
[22] J. E. Medvedeva, M. A. Korotin, V. I. Anisimov, and A. J. Freeman, Phys. Rev. B **65**, 172413 (2002).
[23] For example, in the case of $KCuF_3$ (Ref. 20) all magnetic ordered structures were found to be insulating (as the experimental AF-*A* and PM phases) with comparable band gaps, whereas the nonmagnetic structure was found to be metallic. It is thus more appropriate to use either an ordered magnetic state (e.g., AF-*A*)

which at least satisfies Hund's rule (Ref. 21), or an average of several different spin-ordered states, as has been done in Ref. 22 (no atomic relaxation).

[24] Ideally, the most accurate approach to model the PM state would be the LDA+dynamical mean field theory (LDA+DMFT) approach. In practice, however, an *ab initio* structural optimization study of $LaMnO_3$ as function of pressure is presently beyond the reach of LDA+DMFT calculations.

[25] K. Held, G. Keller, V. Eyert, D. Vollhardt, and V. I. Anisimov, Phys. Rev. Lett. **86**, 5345 (2001).

[26] J. B. A. A. Elemans, B. van Laar, K. R. van der Veen, and B. O. Loopstra, J. Phys. Chem. Solids **3**, 238 (1971).

[27] M. O'Keeffe and B. G. Hyde, Acta Crystallogr., Sect. B: Struct. Crystallogr. Cryst. Chem. **33**, 3802 (1977).

[28] The inclusion of the $4f$ channel (see Ref. 8) has not been found sufficient to obtain a tilted structure.

[29] W. E. Pickett and D. J. Singh, Phys. Rev. B **53**, 1146 (1996).

[30] This leads to vanishing JT distortion at very low pressure (<6 GPa) and a poor description of the structural properties under pressure.

[31] A. Rohrbach, J. Hafner, and G. Kresse, Phys. Rev. B **69**, 075413 (2004).

[32] T. Mizokawa, D. I. Khomskii, and G. A. Sawatzky, Phys. Rev. B **60**, 7309 (1999).

[33] P. Ravindran, A. Kjekshus, H. Fiellvåg, A. Delin, and O. Eriksson, Phys. Rev. B **65**, 064445 (2002).

[34] Q. Qian, T. A. Tyson, S. Savrassov, C.-C. Kao, and M. Croft, Phys. Rev. B **68**, 014429 (2003).

[35] S. Satpathy, Z. Popovic, and F. R. Vukajlovic, Phys. Rev. Lett. **76**, 960 (1996).

[36] D. D. Sarma, N. Shanthi, S. R. Barman, N. Hamada, H. Sawada, and K. Terakura, Phys. Rev. Lett. **75**, 1126 (1995).

[37] S. Baroni, A. dal Corso, S. de Gironcoli, and P. Giannozzi, URL http://www.pwscf.org/.